

Iterative algorithm versus analytic solutions of the parametrically driven dissipative quantum harmonic oscillator

Michael Thorwart, Peter Reimann, and Peter Hänggi

Institut für Physik - Universität Augsburg, Universitätsstr. 1, 86135 Augsburg, Germany

(Date: February 1, 2008)

We consider the Brownian motion of a quantum mechanical particle in a one-dimensional parabolic potential with periodically modulated curvature under the influence of a thermal heat bath. Analytic expressions for the time-dependent position and momentum variances are compared with results of an iterative algorithm, the so-called quasiadiabatic propagator path integral algorithm (QUAPI). We obtain good agreement over an extended range of parameters for this *spatially continuous* quantum system. These findings indicate the reliability of the algorithm also in cases for which analytic results may not be available *a priori*.

PACS: 02.70.-c, 05.30.-d, 05.40.-a

I. INTRODUCTION

Exactly solvable systems have a special status among physical models. Although oversimplified in many cases, they may serve as starting point for testing the reliability of methods which can then be transferred to more realistic, but only numerically solvable models. An important class of such models are quantum systems coupled to a dissipative environment and being driven by a time-dependent external field [1]. A wide variety of physical phenomena have been described by this kind of models, e.g. electron [2] and proton [3] transfer, tunneling processes of a macroscopic spin [4], hydrogen tunneling in condensed phases [5], single defect tunneling in mesoscopic quantum wires [6], or tunneling of the magnetic flux in a SQUID [7], to name but a few. Usually such dissipative quantum systems consist of a model Hamiltonian bilinearly coupled to a bath of harmonic oscillators. Additional external time dependent driving fields render the mathematical solution even more difficult or even impossible.

One of the few analytically tractable time-dependent dissipative quantum systems is the parametrically driven harmonic oscillator whose analytic solution was found by Zerbe and Hänggi in Ref. [8]. A physical realization of this model is the Paul trap [9], which provides an oscillating quadrupole potential for the enclosed ion. Furthermore, the parametrically driven dissipative harmonic oscillator may serve as a benchmark for approximation schemes which were developed for more general dissipative systems [10]. The interesting feature is that the parametric driving induces a non-trivial quasienergy spectrum [10], in contrast to additive driving where the quasienergy spectrum coincides with the spectrum of the undriven system apart from a constant shift. This is further corroborated by the fact that the solution of the parametrically driven linear oscillator can be utilized to obtain solutions of certain nonlinear dynamical systems [11].

Powerful approximative numerical procedures for simulating dissipative and possibly time-dependent quantum systems are the Quantum Monte Carlo method [12] and the quasiadiabatic propagator path integral algorithm (QUAPI) developed by Makri and Makarov [13]. The former method works very well for problems involving path integrals in imaginary time, however, the calculation of real time path integrals is afflicted by the so called *sign-problem* due to the rapidly oscillating integrand. The QUAPI algorithm has been applied to low dimensional dissipative systems such as the driven spin-1/2-particle coupled to a harmonic oscillator bath (driven spin-Boson-system) [13] and to the driven double-well potential in order to study quantum hysteresis and quantum stochastic resonance [14,15]. Moreover, the QUAPI algorithm has recently been used as a basis for a very efficient memory equation algorithm for spin-boson-models [16].

The purpose of this paper is to apply the QUAPI algorithm to the parametrically driven harmonic oscillator and to compare the results with the analytic solution from Ref. [8]. Whilst harmonic oscillator systems are known to exhibit some untypical features this is not the case with respect to the QUAPI algorithm. Our results thus show that not only intrinsically discrete models like the spin-boson-system but also *spatially continuous* systems can be accurately described by few energy eigenstates if the temperature is restricted to a moderate regime. Most importantly, this is the first work in which the numerical approximative QUAPI results are compared against *analytic* solutions of a *spatially continuous* driven dissipative quantum system.

The paper is organized as follows: In section II, we introduce our model of the parametrically driven dissipative quantum harmonic oscillator and briefly review the analytic solution given in Ref. [8]. Section III is devoted to a short review of the QUAPI method. The comparative main results are presented in section IV, before we give the conclusions in section V.

II. THE MODEL AND ITS ANALYTIC SOLUTION

In this section we briefly review the analytic solution of the parametrically driven dissipative harmonic oscillator from [8].

A quantum particle with mass M , position operator \mathbf{x} and momentum operator \mathbf{p} moving in a one-dimensional harmonic potential with periodically modulated curvature is described by the Hamiltonian

$$\mathbf{H}_S(t) = \frac{\mathbf{p}^2}{2M} + \frac{M}{2}[\omega_0^2 + \epsilon \cos \Omega t] \mathbf{x}^2. \quad (1)$$

Following the common approach [1] to model the influence of the environment by an ensemble of harmonic oscillators, the bath Hamiltonian \mathbf{H}_B (including the interaction with the system) is given by

$$\mathbf{H}_B = \sum_j \mathbf{H}_j(\mathbf{x}) = \sum_j \frac{1}{2} \left[\frac{\mathbf{p}_j^2}{m_j} + m_j \omega_j^2 \left(\mathbf{q}_j - \frac{c_j}{m_j \omega_j^2} \mathbf{x} \right)^2 \right], \quad (2)$$

and the whole system is described by the Hamiltonian $\mathbf{H}(t) = \mathbf{H}_S(t) + \mathbf{H}_B$. In the case of a thermal equilibrium bath, it turns out that its influence on the system is fully characterized by the spectral density

$$J(\omega) = \frac{\pi}{2} \sum_j \frac{c_j^2}{m_j \omega_j} \delta(\omega - \omega_j). \quad (3)$$

With the number of harmonic oscillators going to infinity, we arrive at a continuous spectral density. In the following, we choose for the sake of definiteness a truncated Ohmic spectral density, i.e.

$$J(\omega) = M\gamma\omega f_c(\omega, \omega_c). \quad (4)$$

Here, γ is the coupling strength to the heat bath and $f_c(\omega, \omega_c)$ denotes a cut-off function which avoids unphysical divergences due to high-frequency bath modes. For our calculations, we consider two examples for the cut-off function: (i) a smooth exponential cut-off

$$f_c(\omega, \omega_c) = \exp(-\omega/\omega_c) \quad (5)$$

and (ii) a step-function

$$f_c(\omega, \omega_c) = \Theta(\omega_c - \omega) \quad (6)$$

with cut-off frequency $\omega_c \gg \omega_0, \Omega$ (see discussion given below).

We choose a factorizing initial condition of Feynman-Vernon form [17] which means that at time $t = t_0$, the full density operator $\mathbf{W}(t_0)$ is given as a product of the initial system density operator $\rho_S(t_0)$ and the canonical bath density operator at temperature $T = 1/k_B\beta$, i.e.,

$$\mathbf{W}(t_0) = \rho_S(t_0) Z_B^{-1} \exp(-\beta \mathbf{H}_B^0), \quad (7)$$

where $Z_B^{-1} = \text{Tr} \exp(-\beta \mathbf{H}_B^0)$ and

$$\mathbf{H}_B^0 = \sum_j \frac{1}{2} \left[\frac{\mathbf{p}_j^2}{m_j} + m_j \omega_j^2 \mathbf{q}_j^2 \right]. \quad (8)$$

By way of integrating out the bath degrees of freedom in Eq. (2) one obtains the following one-dimensional Heisenberg equation for the position operator \mathbf{x} , i.e.

$$\ddot{\mathbf{x}}(t) + \int_{t_0}^t \hat{\gamma}(t-t') \dot{\mathbf{x}}(t') dt' + (\omega_0^2 + \epsilon \cos \Omega t) \mathbf{x}(t) = \frac{1}{M} \Gamma(t) - \hat{\gamma}(t-t_0) \mathbf{x}(t_0), \quad (9)$$

with the friction kernel given by

$$\hat{\gamma}(t) = \frac{2}{M\pi} \int_0^\infty d\omega \frac{J(\omega)}{\omega} \cos(\omega t). \quad (10)$$

$\Gamma(t)$ is a time-dependent fluctuating (operator) force

$$\Gamma(t) = \sum_j c_j \left(\frac{\mathbf{p}_j(t_0)}{m_j \omega_j} \sin(\omega_j(t - t_0)) + \mathbf{q}_j(t_0) \cos(\omega_j(t - t_0)) \right) \quad (11)$$

which contains the initial conditions of the bath and of the particle's position at time t_0 . The last term on the r.h.s. (proportional to $\mathbf{x}(t_0)$) in Eq. (9) is the so-called initial slip, caused by the specific choice (7) of the initial conditions.

Exploiting the thermal distribution of the bath one recovers the usual connection (via $J(\omega)$) between the random and the frictional forces of the bath in Eq. (11) in the form of the fluctuation-dissipation-relation, reading, $t \geq t'$,

$$\langle \Gamma(t) \Gamma(t') \rangle_\beta = Tr \left[Z_B^{-1} \exp(-\beta \mathbf{H}_B^0) \Gamma(t) \Gamma(t') \right] = \hbar L(t - t') , \quad (12)$$

$$L(t) = \frac{1}{\pi} \int_0^\infty d\omega J(\omega) \left[\coth \left(\frac{\hbar \omega \beta}{2} \right) \cos(\omega t) - i \sin(\omega t) \right] , \quad (13)$$

where the subscript β indicates thermal averaging performed with the canonical density operator for \mathbf{H}_B^0 defined in Eq. (8). The response function $L(t)$ will play an important role in the numerical QUAPI algorithm.

It turns out [8] that for the description of the parametric dissipative quantum oscillator the solution of the classical *deterministic* limit ($\hbar \rightarrow 0, T \rightarrow 0$) with $\omega_c \rightarrow \infty$ plays a prominent role. Thus, in Eq. (9) the position operator \mathbf{x} is replaced by the classical coordinate x and $\int_{t_0}^t \hat{\gamma}(t - t') \dot{\mathbf{x}}(t') dt'$ goes over into $\gamma \dot{x}(t)$. Moreover, on the right hand side of Eq. (9), the fluctuations $\Gamma(t)$ are zero and the initial slip is also omitted, which can be achieved by either a somewhat different choice of the initial conditions than in Eq. (7) or by replacing the coupling coefficients c_j in Eq. (2) by $c_j \Theta(t - t_0^+)$ so that \mathbf{H}_B and \mathbf{H}_B^0 from Eq. (8) coincide at $t = t_0$. For convenience we furthermore introduce scaled quantities

$$\begin{aligned} \tilde{t} &= \frac{\Omega}{2} t, & \tilde{x}(\tilde{t}) &= \sqrt{M\Omega/2\hbar} x(t = \frac{2\tilde{t}}{\Omega}), & \tilde{\omega}_0 &= \frac{2}{\Omega} \omega_0, \\ \tilde{\epsilon} &= \frac{2}{\Omega^2} \epsilon, & \tilde{\gamma} &= \frac{2}{\Omega} \gamma, & \tilde{T} &= \frac{2k_B}{\hbar\Omega} T, & \tilde{\omega}_c &= \frac{2}{\Omega} \omega_c. \end{aligned} \quad (14)$$

In the remainder of this paper, *we exclusively use dimensionless quantities* but omit all the tildes for the sake of better readability. In order to recover the dimensionful quantities, one has to re-introduce tildes wherever it makes sense and then exploit Eq. (14). By substituting $x(t) = y(t) \exp[-\gamma(t - t_0)/2]$ we arrive at an undamped oscillator equation for y which is the well-known Mathieu equation

$$\ddot{y}(t) + (\omega_0^2 - \frac{\gamma^2}{4} + 2\epsilon \cos 2t) y(t) = 0 . \quad (15)$$

Its mathematical properties like stability and instability regions in the parameter space are well known [18]. Nevertheless, there exists no closed analytic expression for the solution and the equation has to be integrated numerically. In the following, we will need two linear independent solutions $\Phi_i(t), i = 1, 2$, of Eq. (15) belonging to two different sets of initial conditions

$$\begin{aligned} \Phi_1(t_0) &= 0, & \dot{\Phi}_1(t_0) &= 1, \\ \Phi_2(t_0) &= 1, & \dot{\Phi}_2(t_0) &= 0. \end{aligned}$$

They can be determined numerically, e.g. by means of a regular fourth-order Runge-Kutta integration of the Mathieu equation (15).

Let us return to the dissipative quantum parametric oscillator. The quantities of interest are the variances of the position and the momentum operator, i.e.

$$\begin{aligned} \sigma_{xx}(t) &\equiv \langle \mathbf{x}^2(t) \rangle - \langle \mathbf{x}(t) \rangle^2, \\ \sigma_{xp}(t) &\equiv \frac{1}{2} \langle \mathbf{x}(t) \mathbf{p}(t) + \mathbf{p}(t) \mathbf{x}(t) \rangle - \langle \mathbf{x}(t) \rangle \langle \mathbf{p}(t) \rangle, \\ \sigma_{pp}(t) &\equiv \langle \mathbf{p}^2(t) \rangle - \langle \mathbf{p}(t) \rangle^2. \end{aligned} \quad (16)$$

Here, the quantum mechanical expectation value is understood as usual as $\langle \cdot \rangle = \text{Tr}[\rho(t) \cdot]$. By determining the propagator $\mathbf{U}(t, t_0) = \mathcal{T} \exp(-i \int_{t_0}^t dt' \mathbf{H}(t')/\hbar)$ (\mathcal{T} is the time ordering operator) for the driven dissipative system according to [8], the reduced density matrix $\rho(t) = \text{Tr}_{\text{Bath}}(\mathbf{U}(t, t_0) \mathbf{W}(t_0) \mathbf{U}^{-1}(t, t_0))$ can be calculated analytically. Here, $\mathbf{W}(t_0)$ denotes the full density operator at time t_0 and Tr_{Bath} the trace over the bath degrees of freedom. Having obtained the reduced density operator $\rho(t)$, the quantum mechanical expectation values in Eq. 16) can be evaluated. After some algebra, we find for the dimensionless variances the expressions

$$\sigma_{xx}(t) = e^{-\gamma(t-t_0)} \left\{ [\Phi_2(t) - \frac{\gamma}{2} \Phi_1(t)]^2 \sigma_{xx}^0 + 2\Phi_1(t) [\Phi_2(t) - \frac{\gamma}{2} \Phi_1(t)] \sigma_{xp}^0 + \Phi_1^2(t) \sigma_{pp}^0 \right\} + \Sigma_{xx}(t), \quad (17a)$$

$$\sigma_{xp}(t) = \frac{1}{2} \dot{\sigma}_{xx}(t), \quad (17b)$$

$$\sigma_{pp}(t) = \dot{\sigma}_{xp}(t) + \gamma \sigma_{xp}(t) + [\omega_0^2 + 2\epsilon \cos(2t)] \sigma_{xx}(t) - \Sigma_{pp}(t). \quad (17c)$$

Thereby, we have rectified [19] some minor misprints in [8] and simplified the equations in [8] for σ_{xp} and σ_{pp} . Here, $\sigma_{xx}^0, \sigma_{xp}^0$ and σ_{pp}^0 denote the initial variances of the *uncoupled* system at time $t = t_0$ which depend on the choice of the initial state for the bare system $\mathbf{H}_S(t_0)$. The initial conditions for Eqs. (17) at time $t = t_0^+$ are given by

$$\begin{aligned} \sigma_{xx}(t_0^+) &= \sigma_{xx}^0, \\ \sigma_{xp}(t_0^+) &= -\gamma \sigma_{xx}^0 + \sigma_{xp}^0, \\ \sigma_{pp}(t_0^+) &= \gamma^2 \sigma_{xx}^0 - 2\gamma \sigma_{xp}^0 + \sigma_{pp}^0. \end{aligned} \quad (18)$$

The discontinuity of the variances at time t_0 is a well-known consequence [1] of the initial slip term in Eq. (9); it is due to the factorizing initial condition (7). The first terms in the three equations (17) possess the same form as in the classical case. The specific quantum mechanical features enter via the functions $\Sigma_{xx}(t)$ and $\Sigma_{pp}(t)$, which read

$$\begin{aligned} \Sigma_{xx}(t) &= \frac{\gamma}{\pi} \int_0^\infty d\omega \omega f_c(\omega, \omega_c) \coth\left(\frac{\omega}{2T}\right) \left\{ \left[\int_{t_0}^t ds G(t, s) \exp\left(\frac{\gamma}{2}(t-s)\right) \cos(\omega s) \right]^2 \right. \\ &\quad \left. + \left[\int_{t_0}^t ds G(t, s) \exp\left(\frac{\gamma}{2}(t-s)\right) \sin(\omega s) \right]^2 \right\}, \end{aligned} \quad (19a)$$

$$\Sigma_{pp}(t) = \frac{\gamma}{\pi} \int_0^\infty d\omega \omega f_c(\omega, \omega_c) \coth\left(\frac{\omega}{2T}\right) \int_{t_0}^t ds G(t, s) \exp\left(\frac{\gamma}{2}(t-s)\right) \cos(\omega(t-s)), \quad (19b)$$

where $G(t, s) = \Phi_1(t)\Phi_2(s) - \Phi_1(s)\Phi_2(t)$. While in Eq. (19) a general form of the cut-off function $f_c(\omega, \omega_c)$ with $\omega_c \gg \omega_0$ is kept, the analytic solution (17) is based [8] on the assumption of a strictly Ohmic classical dynamics ($\omega_c \rightarrow \infty$) in Eq. (10). The consequence of this assumption is the discontinuity at $t = t_0$ in Eq. (18) when the system-bath-interaction is switched on instantaneously. A finite cut-off in the spectral density $J(\omega)$ in the damping kernel (10) would induce a smooth time evolution of the variances (17) close to $t = t_0$ on a time scale ω_c^{-1} .

The relations (17, 19) are evaluated by standard numerical methods. The efficiency is improved if one applies Floquet's theorem for the fundamental solutions $\Phi_j(s)$. Then, the periodic part of the Floquet solutions can be expanded in a Fourier series and the integrations over the intermediate times s in Eq. (19) can be performed analytically. Finally, the remaining ω -integrations and the sum over the Fourier modes can be readily carried out.

III. NUMERICAL SOLUTION WITH REAL-TIME PATH INTEGRALS

In the following section, we recapitulate the essentials of the QUAPI algorithm. Further details can be found in the original works by Makri and Makarov [13]. In order to describe the dynamics of the system of interest it is sufficient to consider the time evolution of the elements of the reduced density matrix which reads in position representation

$$\begin{aligned} \rho(x_f, x'_f; t_f) &= \text{Tr}_{\text{Bath}} \langle x_f \Pi_j q_j | \mathbf{U}(t_f, t_0) \mathbf{W}(t_0) \mathbf{U}^{-1}(t_f, t_0) | x'_f \Pi_j q'_j \rangle, \\ \mathbf{U}(t_f, t_0) &= \mathcal{T} \exp \left\{ -i/\hbar \int_{t_0}^{t_f} \mathbf{H}(t') dt' \right\}. \end{aligned} \quad (20)$$

Here, \mathcal{T} denotes the chronological operator, $\mathbf{W}(t_0)$ the full density operator at the initial time t_0 and Tr_{Bath} the partial trace over the harmonic bath oscillators q_j . Due to our assumption that the bath is initially at thermal

equilibrium and decoupled from the system, $\mathbf{W}(t_0)$ becomes the product of the initial system density operator $\rho_S(t_0)$ and the canonical bath density operator at temperature T , see Eq. (7). Then, the partial trace over the bath can be performed and the reduced density operator be rewritten according to Feynman and Vernon [17] as

$$\rho(x_f, x'_f, t_f) = \int dx_0 dx'_0 G((x_f, x'_f, t_f; x_0, x'_0, t_0) \rho(x_0, x'_0, t_0) , \quad (21)$$

with the propagator G given by

$$G(x_f, x'_f, t_f; x_0, x'_0, t_0) = \int \mathcal{D}x \mathcal{D}x' \exp \left\{ \frac{i}{\hbar} (S_S[x] - S_S[x']) \right\} \mathcal{F}_{FV}[x, x'] . \quad (22)$$

$S_S[x]$ is the classical action functional of the system-variable x along a path $x(t)$ and $\mathcal{F}_{FV}[x, x']$ denotes the Feynman-Vernon influence functional

$$\mathcal{F}_{FV}[x, x'] = \exp \left\{ -\frac{1}{\hbar} \int_{t_0}^{t_f} dt \int_t^{t_f} dt' [x(t') - x'(t')] [\eta(t' - t)x(t) - \eta^*(t' - t)x'(t)] \right\} , \quad (23)$$

with the integral kernel

$$\eta(t) = L(t) + i\delta(t) \frac{2}{\pi} \int_0^\infty \frac{d\omega}{\omega} J(\omega) \quad (24)$$

and the autocorrelation function $L(t)$ given in Eq. (13). As usual, the restriction to paths that satisfy the boundary conditions $x_0(t_0) = x_0$, $x_f(t_f) = x_f$ and similarly for $x'(t)$ is understood implicitly in Eq. (22). Likewise, the dependence of the density operator ρ in Eq. (21) on the initial time t_0 and on $\rho_S(t_0)$ has been dropped.

To make the equations numerically tractable, we discretize $t_f - t_0$ into N steps Δt , such that $t_k = t_0 + k\Delta t$ and split the full propagator over one time step $\mathbf{U}(t_{k+1}, t_k)$ in Eq. (20) according to the Trotter formula symmetrically into a system and an environmental part:

$$\begin{aligned} \mathbf{U}(t_{k+1}, t_k) &\approx \exp(-i\mathbf{H}_B\Delta t/2\hbar) \mathbf{U}_S(t_{k+1}, t_k) \exp(-i\mathbf{H}_B\Delta t/2\hbar) , \\ \mathbf{U}_S(t_{k+1}, t_k) &= \mathcal{T} \exp \left\{ -\frac{i}{\hbar} \int_{t_k}^{t_{k+1}} dt' \mathbf{H}_S(t') \right\} . \end{aligned} \quad (25)$$

The symmetric splitting of the propagator in Eq. (25) causes an error proportional to Δt^3 . This error will be studied in detail in section IV below. The short-time propagator \mathbf{U}_S of the bare system is numerically evaluated by means of a Runge–Kutta scheme with adaptive step-size control. Exploiting the approximation (25), the propagator in the position representation now factorizes as

$$\langle x \Pi_j q_j | \mathbf{U}(t_{k+1}, t_k) | x' \Pi_j q'_j \rangle \approx \langle x | \mathbf{U}_S(t_{k+1}, t_k) | x' \rangle \prod_j \langle q_j | e^{-i\mathbf{H}_j(x)\Delta t/2\hbar} e^{-i\mathbf{H}_j(x')\Delta t/2\hbar} | q'_j \rangle , \quad (26)$$

where the $\mathbf{H}_j(x)$ are defined in Eq. (2). By exploiting this approximation and performing the partial trace over the bath modes in Eq. (20), one recovers Eq. (21), but now with a discretized version of the propagating function (22), i.e.,

$$\begin{aligned} \rho(x_f, x'_f, t_f) &= \int dx_0 \dots \int dx_N \int dx'_0 \dots \int dx'_N \delta(x'_f - x'_N) \delta(x_f - x_N) \\ &\times \langle x_N | \mathbf{U}_S(t_f, t_f - \Delta t) | x_{N-1} \rangle \dots \langle x_1 | \mathbf{U}_S(t_0 + \Delta t, t_0) | x_0 \rangle \\ &\times \langle x_0 | \rho_S(t_0) | x'_0 \rangle \langle x'_0 | \mathbf{U}_S^{-1}(t_0 + \Delta t, t_0) | x'_1 \rangle \dots \langle x'_{N-1} | \mathbf{U}_S^{-1}(t_f, t_f - \Delta t) | x'_N \rangle \\ &\times \mathcal{F}_{FV}^{(N)}(x_0, x'_0, \dots, x_N, x'_N) . \end{aligned} \quad (27)$$

Here, $\mathcal{F}_{FV}^{(N)}(x_0, \dots, x'_N)$ is the discrete Feynman–Vernon influence functional (23) where the paths $x(t)$ and $x'(t)$ consist of constant segments x_k and x'_k , respectively, within each time interval $t_k - \frac{1}{2}\Delta t < t_k < t_k + \frac{1}{2}\Delta t$ and can be rewritten in the form

$$\mathcal{F}_{FV}^{(N)}(x_0, \dots, x'_N) = \exp \left\{ -\frac{1}{\hbar} \sum_{k=0}^N \sum_{k'=k}^N [x_{k'} - x'_k] [\eta_{k'k} x_k - \eta_{k'k}^* x'_k] \right\} . \quad (28)$$

The coefficients $\{\eta_{k'k}\}$ are closely related to their continuous time counterpart $\eta(t)$ in Eq. (24). Their explicit form is lengthy and not very illuminating for our purposes; their detailed form can be looked up in Ref. [13].

To make further progress, it is necessary to approximately break the influence kernel $\mathcal{F}_{FV}^{(N)}(x_0, \dots, x'_N)$ in Eq. (28) into smaller pieces. To this end, Makri and Makarov use the fact [20,13] that the real part of the integral kernel $L_R(t)$ typically exhibits a pronounced peak at $t = 0$, and quickly approaches 0 for $t \rightarrow \pm\infty$. The decay to zero depends naturally on the choice of the cut-off function $f_c(\omega, \omega_c)$, see Eq. (4). This suggests the truncation of $\eta(t)$ after a certain number K of time steps Δt and, correspondingly, to neglect $\eta_{k'k}$ if $k' > k + K$, i.e.

$$\mathcal{F}_{FV}^{(N)}(x_0, \dots, x'_N) \approx \prod_{k=0}^N \prod_{k'=k}^{\min\{N, k+K\}} \exp \left\{ -\frac{1}{\hbar} [x_{k'} - x'_{k'}] [\eta_{k'k} x_k - \eta_{k'k}^* x'_k] \right\}. \quad (29)$$

In doing so, we approximate $L(t)$ by zero for $t > K\Delta t$, cf. Eqs. (13, 24). Of course, this truncation induces an error in the final result which has to be handled with care. The error becomes increasingly less important for increasing temperatures since then, the bath-induced correlations fall off increasingly faster. In other words, for higher temperatures the width of the response function $L(t)$ decreases. In the other limit of decreasing temperature however, the number K of relevant time-intervals is increasing and in the limit of zero temperature $T = 0$, it is well known [1] that the response function $L(t)$ falls off only algebraically for $t \rightarrow \pm\infty$. Nevertheless, we will see that this approach allows to deal with quite low temperatures and produces qualitative agreement with analytic solutions.

The next goal is to approximate the spatially continuous integrals in Eq. (27) in terms of finite sums. To this end, Makri and Makarov perform a transformation into a basis given by the energy eigenstates $|\phi_m\rangle$ of the bare system Hamiltonian $\mathbf{H}_S(t_r)$ (1), but with the driving term clamped to an appropriate but fixed (!) reference time t_r , i.e.

$$\mathbf{H}_S(t_r)|\phi_m\rangle = E_m|\phi_m\rangle, \quad m = 1, 2, \dots. \quad (30)$$

E_m denotes the energy eigenvalues of the static system Hamiltonian $\mathbf{H}_S(t_r)$. In certain cases, symmetry properties suggest the choice of an appropriate t_r . Here, we choose the unperturbed harmonic oscillator as a reference configuration. This means for our choice of driving to use $t_r = \pi/4$, so that $\cos(2t_r) = 0$ in Eq. (15). Reintroducing now the thermal bath but restricting ourselves to small-to-moderate temperatures T , the thermal occupation of high energy levels E_m is expected to be negligible. This argument suggests that the $|\phi_m\rangle$ provide a well adapted basis admitting a fast convergent truncation scheme. In other words, we may approximately project the dynamics onto the Hilbert subspace spanned by the first few energy eigenstates $|\phi_m\rangle$, $m = 1, \dots, M$, corresponding to an approximate decomposition of the identity operator $\mathbb{I} \approx \sum_{m=1}^M |\phi_m\rangle\langle\phi_m|$. Before doing so, we perform one more unitary transformation within that M -dimensional Hilbert space such that the position operator becomes diagonal [discrete variable representation, DVR [21]]:

$$|u_m\rangle = \sum_{m'=1}^M R_{mm'} |\phi_{m'}\rangle, \quad \langle u_m | \mathbf{x} | u_{m'} \rangle = x_m^{DVR} \delta_{mm'}, \quad m, m' = 1, \dots, M. \quad (31)$$

Exploiting the approximate decomposition of the identity $\mathbb{I} \approx \sum_{m=1}^M |u_m\rangle\langle u_m|$ and the truncation of the bath-induced correlations in Eq. (29), it is a matter of straightforward but tedious manipulations – starting from Eq. (27) – to arrive at the final form of the QUAPI recursion scheme. In particular, the integrals in Eq. (27) turn into finite sums due to the transformation (31) into the DVR-basis. We do not present the detailed form here and refer the reader again to the original literature [13].

The above introduced restriction to a finite dimensional subspace induces an error in the evaluation of the reduced density matrix. However, as we will also discuss below, this error behaves in a controlled way if the relevant parameters such as the temperature and the damping are chosen in a moderate regime. This means that for increasing temperature increasingly more DVR-states are necessary to describe the dynamics appropriately. Note that in this regime however, the number K of the relevant memory time steps is decreasing. In the opposite limit of decreasing temperature, the number M of relevant basis states can be chosen rather small. In this low-temperature limit the number K of memory time steps can therefore be increased. Moreover, we note that the restriction of the dynamics (at long times) to the M -dimensional Hilbert subspace is not allowed for systems with an inherent diverging dynamics. This is also seen in our example of the parametrically driven dissipative quantum harmonic oscillator for a parameter choice in an instability region of the Mathieu equation (15), see section IV below.

The efficiency of the QUAPI algorithm is based on the choice of the two free parameters M (the number of basis states) and K (the length of the memory). The numerical objects that one has to deal with are arrays of size M^{2K+2} and M^{2K} . In practice, the calculations have been performed on conventional IBM RS/6000 workstations (43P-260 and 3CT). The computation time for an iteration over a typical time span $[0, 40]$ depends strongly on the chosen

parameters. It ranges from several milliseconds for $M = 3, K = 2$ (program size 7 MB) over several seconds for $M = 3, K = 4$ (program size 8 MB) up to several hours for $M = 5, K = 4$ (program size 176 MB). The strongly limiting factor is the program size since the size of the arrays grows exponentially with K . E.g., the parameter combination $M = 4, K = 6$ leads to too large arrays and cannot be treated by standard programming techniques. In practice, with the choice $M = 6, K = 3$ or $M = 5, K = 4$, we already are at the upper limit of the QUAPI algorithm.

IV. RESULTS

We proceed in reporting our results for the specific example of the parametrically driven dissipative quantum harmonic oscillator. With the reduced density matrix (27) at hand, we can calculate the variances (16) within the QUAPI algorithm and compare them with the analytic predictions (17,19). Most of the figures contain results for rather extreme parameter values, e.g. low temperature and large driving amplitude, in order to show that the QUAPI algorithm performs satisfactorily also in these limits. For more moderate choices of the parameters, the agreement (not shown) between numerical and analytic results is much better.

Our main goal is to study the dependence of the variances (16) on the QUAPI parameters M, K and Δt . For finite M and K , the deviation increases proportional to Δt^3 due to the Trotter splitting in Eq. (25) with increasing Δt . For decreasing Δt , the Trotter error decreases but the error made by the memory truncation in Eq. (29) starts to dominate since more and more bath correlations are neglected. Thus, the overall error increases again. In between there exists an “optimal time step of least dependence”, where the quantities are least sensitive to variations of Δt . This represents the “principle of minimal sensitivity” for the optimal choice of the time step Δt for the QUAPI algorithm (see also [16]). For M finite and $K \rightarrow \infty$, the result would be independent of Δt for small Δt since the Trotter error would vanish and also the finite-memory error would not exist.

The choice of M and K should be adapted to the chosen bath parameters. In the case of no driving, if the temperature is low, only few energy eigenstates are required, i.e. M may be chosen small. However, low temperature induces long-range bath correlations. Therefore, the memory length K has to be assumed large. The opposite holds true in the other limit of high temperature. In the case of driving, the number M of basis states is more important compared to the undriven case, since the variances oscillate strongly and higher lying energy states are excited. The memory length K has to be reduced instead if one is interested in the oscillation amplitudes. However, for the mean value of the variances, the total memory length K is again more important and should be maximized (see below).

We shall choose two representative parameter sets for our considerations. Since the memory in Eq. (28) is truncated in the QUAPI algorithm according to Eq. (29), the crucial parameters are the temperature T and the damping strength γ . The relatively high temperature $T = 1.0$ and the small damping $\gamma = 0.1$ form the first parameter set (*High temperature – weak damping*). For this choice, the numerical results are expected to agree well with the analytic results because large T suppresses the long-time memory contributions in Eq. (28) and additionally, a small γ diminishes the influence of the bath correlations (12). Our second parameter set is given by $T = 0.1, \gamma = 1.0$ (*Low temperature – strong damping*). In this case, long-range bath correlations (12) play a major role and the truncation of them will induce an error which will be larger than in the case of a high temperature and weak damping. For intermediate parameter regimes, we find no qualitative differences.

In all our calculations, we set $t_0 = 0$ and choose as the initial state the ground-state of the maximally curved (i.e. $\omega_0^2 \rightarrow \omega_0^2 + 2\epsilon$) harmonic oscillator, i.e. $\rho_S(t_0 = 0) = |0\rangle\langle 0|$. The corresponding initial variances in Eq. (17) readily follow as $\sigma_{xx}^0 = 1/(2\sqrt{\omega_0^2 + 2\epsilon})$, $\sigma_{xp}^0 = 0$ and $\sigma_{pp}^0 = \sqrt{\omega_0^2 + 2\epsilon}/2$. Our standard choice for the cut-off function will be the exponential cut-off (5), if nothing else is stated. Furthermore, we always choose the dimensionless curvature $\omega_0 = 1.0$ in order to have a rather small separation of the energy levels in the undriven oscillator. This induces a high sensitivity on the number M of basis states since the higher lying states are then easily populated thermally or by driving induced transitions. The choice of a larger ω_0 would be more in favour of the numerical algorithm.

A. High temperature – weak damping (no driving)

First, we consider the undriven case $\epsilon = 0$. Fig. 1 depicts the results for a high temperature $T = 1.0$ and small friction $\gamma = 0.1$. Here and in the following, we use the dimensionless quantities which have been introduced in Eq. (14). Moreover, $\omega_0 = 1.0$ and $\omega_c = 50.0$. We find very good agreement with the analytic solution for the variances. The initial transient oscillations are reproduced and the asymptotic values for long times as well. The initial jump of $\sigma_{xp}(t)$ (of Eq. (18)) is still visible, while the jump of $\sigma_{pp}(t)$ is proportional to γ^2 and is not visible on this plot.

To be able to study the dependence of the QUAPI algorithm on the parameters M, K and Δt we consider the asymptotic values of the variances at long times. It is clear from Eq. (19) that $\sigma_{xp}(\infty) = 0$, so we focus in Fig. 2 on the

two non-trivial variances $\sigma_{xx}(\infty)$ and $\sigma_{pp}(\infty)$. The qualitative dependence of both variances on the time step Δt is always similar: The deviation increases with increasing Δt due to the error proportional to Δt^3 in the Trotter splitting in Eq. (25). For decreasing Δt , this error decreases and the “finite-K”-error takes over. The relevant Δt -value on which we focus in the following is the one for which the numerical result varies the least, i.e. the minima in the curves in Fig. 2 (“principle of minimal sensitivity” [16]).

The left column of Fig. 2 confirms that for a fixed memory length $\Delta t \cdot K$, a smaller time step Δt induces a smaller Trotter-error whereas the finite-K-error remains roughly the same. While for a fixed M (left column in Fig. 2) QUAPI tends to underestimate the analytic result as K increases, a fixed K and growing M (right column) leads to an opposite trend, suggesting that indeed the analytic result will be approached best when *both* M and K become large (at a plateau Δt -value tending towards zero).

B. Low temperature – strong damping

1. No driving

Fig. 3 depicts the time-dependence of the variances in satisfactory agreement with the analytic result. The initial jumps of $\sigma_{xp}(t)$ and of $\sigma_{pp}(t)$ are more pronounced in this strong damping case since the jumps are proportional to γ and γ^2 (see Eq. (18)). The deviations in the transient behavior are due to the assumption of a strictly Ohmic classical dynamics (infinite cut-off ω_c) in the analytic solution, see the discussion at the end of section II. They become more pronounced for low temperatures and strong friction because this assumption induces deviations in the short-time evolution of the variances on a time-scale ω_c^{-1} . The bath-induced long-range memory at this low temperature carries the deviations over the whole range of the transient dynamics. The fact that the memory length K is decisive for this low temperature is confirmed by the dashed-dotted line.

The dependence of the asymptotic values $\sigma_{xx}(\infty)$ and $\sigma_{pp}(\infty)$ on the QUAPI parameters is shown in Fig. 4. The number M of basis states is not so important, while the memory length K is decisive. Again, the analytic prediction is correctly approached when both M and K are increased.

2. With driving

Fig. 5 demonstrates for a small driving amplitude reasonable agreement with the analytics. The long-memory parameter set with $K = 6$ hits best the asymptotic mean value, but the oscillation amplitudes and frequencies are obtained best by the choice of a large $M = 5$. In comparison to the undriven case ($\epsilon = 0$) the time averaged variances are almost unchanged (Figs. 4 and 6) while the time-resolved behavior (Figs. 3 and 5) displays notable differences.

Fig. 7 depicts the time evolution for the relatively large driving amplitude. As expected, for strong driving, a large number M of basis states are required to describe the oscillations correctly. The averaged asymptotic values $\bar{\sigma}_{xx}(\infty)$ and $\bar{\sigma}_{pp}(\infty)$ are plotted in Fig. 8. Since the strong driving mixes high energy eigenstates, the results are considerably more sensitive to the choice of M than for weak driving (Fig. 6 upper right panel). However, the same argumentation applies like in the undriven case (see Fig. 4). Considering the rather extreme parameters (small level-spacing, strong driving, low temperature, strong damping) the agreement with the analytic results is still satisfactory.

C. Diverging dynamics and dependence on the cut-off ω_c

Fig. 9 shows $\sigma_{xx}(t)$ for parameters belonging to an instability region of the Mathieu oscillator (15) [18], i.e. the variances for the driven quantum harmonic oscillator diverge for long times. Since the QUAPI algorithm is restricted to a (finite) M -dimensional Hilbert subspace it cannot reproduce such an asymptotic divergence.

The last issue we address is the dependence of the dynamics on the cut-off parameter ω_c and on the explicit *shape* of the cut-off function (5,6). First, we keep an exponential cut-off but choose a smaller cut-off frequency ω_c . It is well known [1] that for the (undriven) quantum harmonic oscillator $\sigma_{pp}(\infty)$ diverges with ω_c , while $\sigma_{xx}(\infty)$ is asymptotically independent of ω_c . In Fig. 10, we choose the “worst” case (i.e. low temperature and strong damping) without driving and decrease the cut-off to $\omega_c = 10.0$. Compared to Fig. 3, the value of $\sigma_{xx}(\infty)$ is indeed practically unchanged while $\sigma_{pp}(\infty)$ has notably decreased.

Fig. 11 shows results for a step-like cut-off (6). First, we observe that mainly the short-time behavior of the relaxation process is affected. Clearly, QUAPI with its restriction to only a few energy eigenstates cannot reproduce the transient high-frequency oscillations of $\sigma_{pp}(t)$. Second, we note that a step-like cut-off affects the decay of the

response function $L(t)$ from Eq. (13) for $t \rightarrow \infty$. The real/imaginary part of $L(t)$ decays qualitatively like an algebraically damped cos/sin-function. While this might suggest a strong dependence of the QUAPI results on the memory length, we actually find a rather weak dependence since the agreement between numeric and analytic results in Fig. 11 is not considerably worse than in Fig. 3. This means that the memory truncation in Eq. (29) is in fact not very sensitive to the choice of the cut-off function $f_c(\omega, \omega_c)$ as long as one is not interested in the detailed short-time behavior.

V. CONCLUSIONS

We have studied the dependence of the QUAPI algorithm on its three numerical parameters, namely the time-step Δt , the number M of basis states, and the memory length K . As a test system, we have used the analytically solvable dissipative quantum harmonic oscillator and its parametrically driven generalization. The comparison shows a decent agreement of the approximative numerical result with the analytic solution, even in the case with driving. This means that a *spatially continuous* system can be described reasonably well by taking only a few basis states and a finite memory length into account. For low temperatures and weak-to-moderate driving, the number M of basis states has to be chosen small and the memory length K large, while in the opposite regime of high temperature, M has to be large but K may be chosen small. In both cases, satisfactorily large M and K values are still numerically feasible. For strong driving, the deviations increase but the QUAPI results are still in qualitative agreement with the analytic predictions.

Our findings demonstrate the reliability of the QUAPI algorithm even in driven, *spatially continuous* systems and not only in finite, discrete dissipative quantum systems such as the spin-Boson-system. Therefore, the QUAPI algorithm may become a standard procedure for simulating open quantum systems in the presence of a novel class of time-dependent, not necessarily periodic driving fields. This technique is especially interesting for the study of decoherence in interacting two-level-systems processing quantum bits. There, the quantum gate operation prescribes the time-dependence of the external control fields which may exhibit a complex non-periodic time-dependence.

ACKNOWLEDGEMENT

This work has been supported by the Deutsche Forschungsgemeinschaft Grant No. HA 1517/19-1 (P.H., M.T.), in part by the Sonderforschungsbereich 486 of the Deutsche Forschungsgemeinschaft (P.H.) and by the DFG-Graduiertenkolleg 283.

-
- [1] U. Weiss, *Quantum Dissipative Systems*, (World Scientific, Singapore, 1993; Second edition 1999).
 - [2] R. A. Marcus, J. Chem. Phys. **43**, 679 (1965); I. Rips and J. Jortner, J. Chem. Phys. **87**, 2090 (1987).
 - [3] S. Nagaoka, T. Terao, F. Imashiro, A. Saika, and N. Hirota, J. Chem. Phys. **79**, 4694 (1983).
 - [4] W. Wernsdorfer, T. Ohm, C. Sangregorio, R. Sessoli, D. Mailly, and C. Paulsen, Phys. Rev. Lett. **82**, 3903 (1999); W. Wernsdorfer and R. Sessoli, Science **284**, 133 (1999).
 - [5] H. Wipf, D. Steinbinder, K. Neumaier, P. Gutsmedl, A. Magerl, and A. J. Dianoux, Europhys. Lett. **4**, 1379 (1987).
 - [6] B. Golding, N. M. Zimmerman, and S. N. Coppersmith, Phys. Rev. Lett. **68**, 998 (1994).
 - [7] S. Han, J. Lapointe, and J. E. Lukens, Phys. Rev. Lett. **66**, 810 (1991).
 - [8] C. Zerbe and P. Hänggi, Phys. Rev. E **52**, 1533 (1995).
 - [9] L. S. Brown, Phys. Rev. Lett. **66**, 527 (1991).
 - [10] S. Kohler, R. Utermann, P. Hänggi, and T. Dittrich, Phys. Rev. E **58**, 7219 (1998).
 - [11] M. Lutzky, Phys. Lett. **68A**, 3 (1978); J. Rezende, J. Math. Phys. **25**, 3264 (1984).
 - [12] K. Binder and D. W. Heermann, *Monte Carlo Simulation in Statistical Physics*, (Springer, Berlin 1988).
 - [13] D. E. Makarov and N. Makri, Chem. Phys. Lett. **221**, 482 (1994); N. Makri and D. E. Makarov, J. Chem. Phys. **102**, 4600 (1995); **102**, 4611 (1995); N. Makri, J. Math. Phys. **36**, 2430 (1995).
 - [14] M. Thorwart and P. Jung, Phys. Rev. Lett. **78**, 2503 (1997); M. Thorwart, P. Reimann, P. Jung, and R.F. Fox, Chem. Phys. **235**, 61 (1998); M. Thorwart, P. Reimann, and P. Jung, Phys. Lett. A **239**, 233 (1998).
 - [15] M. Grifoni and P. Hänggi, Phys. Rev. Lett. **76**, 1611 (1996); Phys. Rev. E **54**, 1390 (1996); Phys. Rep. **304**, 230 (1998).
 - [16] A. A. Golosov, R. A. Friesner, and P. Pechukas, J. Chem. Phys. **110**, 138 (1999).

- [17] R. P. Feynman and F. L. Vernon Jr., Ann. Phys. (N.Y.) **24**, 118 (1963).
- [18] A. H. Nayfeh, D. T. Mook, *Nonlinear Oscillations*, (Wiley, New York, 1979). M. Abramowitz, I. A. Stegun, *Handbook of Mathematical Functions*, (Dover, New York, 1972).
- [19] In eq. (60) in Ref. [8], the factor 1/2 in the σ_{xp}^0 -term has to be omitted. Moreover, in eq. (61), the last term should read correctly $\dots + 2\hbar m(\dot{f}_1^2 a_{11} + 2\dot{f}_1 a_{12} + a_{22})$.
- [20] A. O. Caldeira and A. J. Leggett, Ann. Phys. (N.Y.) **149**, 374 (1983).
- [21] D. O. Harris, G. G. Engerholm, and W. D. Gwinn, J. Chem. Phys. **43**, 1515 (1965).

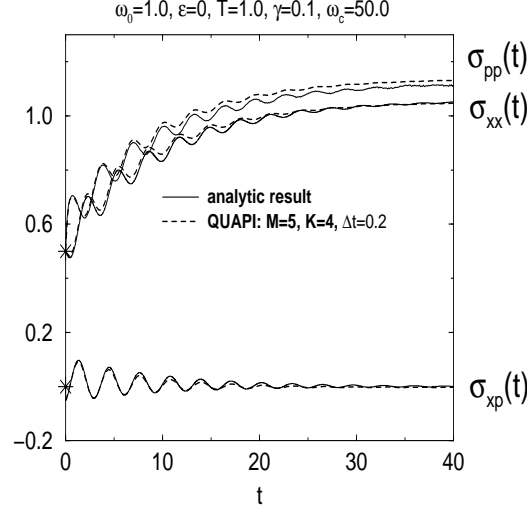


FIG. 1. Time-dependence of the variances $\sigma_{xx}(t)$, $\sigma_{xp}(t)$, and $\sigma_{pp}(t)$ for the undriven dissipative quantum harmonic oscillator ($\epsilon = 0, \omega_0 = 1.0$) with bath parameters $T = 1.0, \gamma = 0.1$ and an exponential cut-off Eq. (5) with $\omega_c = 50.0$. In all the figures, we have used dimensionless quantities according to Eq. (14). The solid lines depict the analytic results (17) while the dashed lines represent the numerical solution obtained by the QUAPI algorithm with $M = 5, K = 4, \Delta t = 0.2$. The asterisks mark the initial variances $\sigma_{xx}^0 = \sigma_{pp}^0 = 0.5$ and $\sigma_{xp}^0 = 0$.

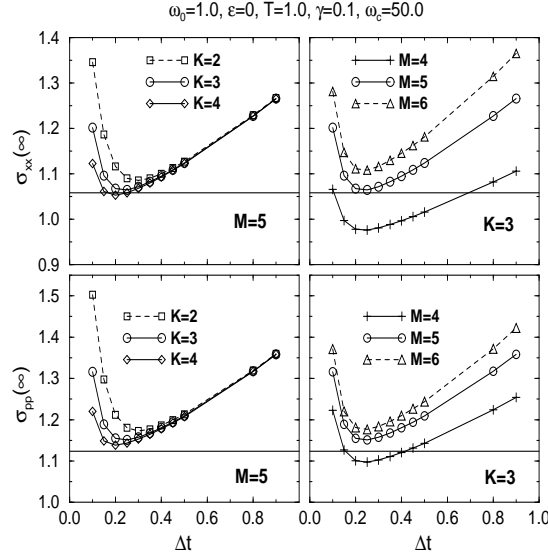


FIG. 2. Asymptotic values of the position (upper row) and momentum (lower row) variances $\sigma_{xx}(\infty)$ and $\sigma_{pp}(\infty)$, respectively, as a function of the time-step Δt and different combinations of the two QUAPI parameters M (number of basis states) and K (number of memory time steps) for the undriven dissipative quantum harmonic oscillator ($\epsilon = 0, \omega_0 = 1.0$) and heat bath parameters $T = 1.0, \gamma = 0.1$ and $\omega_c = 50.0$ with exponential cut-off Eq. (5). For the left column figures, the number M of basis states is fixed to $M = 5$ and the memory length K is varied, while for the right column figures, K is fixed to $K = 3$ and M is varied. Interconnected symbols: solutions obtained by QUAPI. Horizontal solid line: analytic result (17).

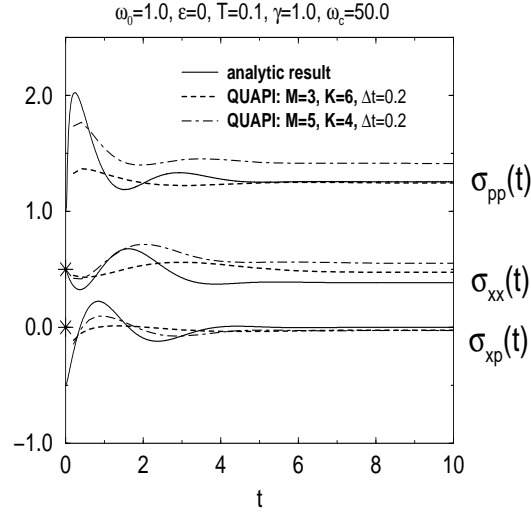


FIG. 3. Same as Fig. 1, but for the parameters $T = 0.1, \gamma = 1.0$. Here, the QUAPI parameters are $M = 3, K = 6, \Delta t = 0.2$ (dashed line) and $M = 5, K = 4, \Delta t = 0.2$ (dashed-dotted line).

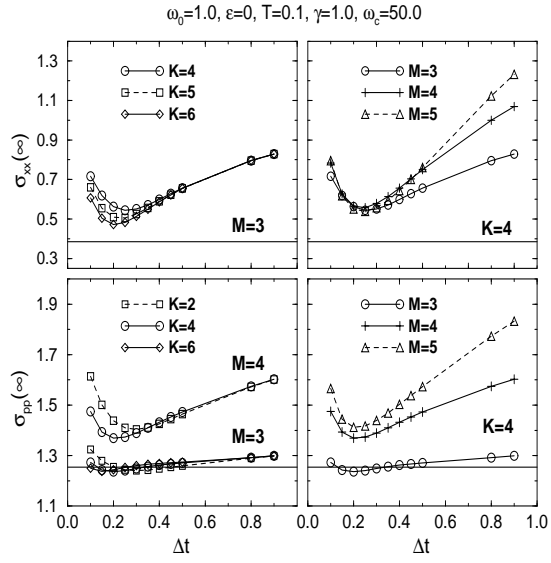


FIG. 4. Same as Fig. 2, but for the bath parameters $T = 0.1, \gamma = 1.0$.

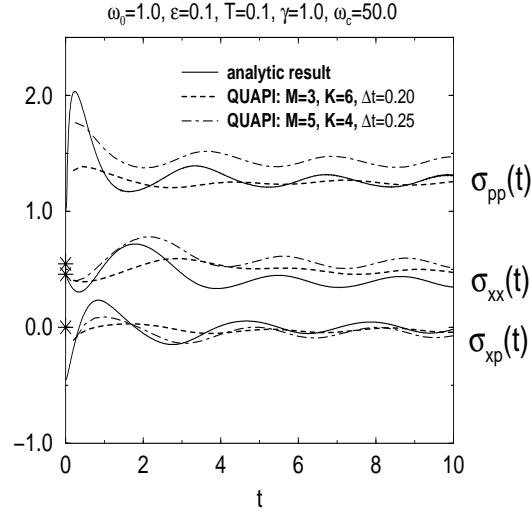


FIG. 5. Time-dependence of the variances $\sigma_{xx}(t)$, $\sigma_{xp}(t)$ and $\sigma_{pp}(t)$ for the parametrically driven dissipative quantum harmonic oscillator with $\omega_0 = 1.0$ and a small driving amplitude $\epsilon = 0.1$. The bath parameters are $T = 0.1$, $\gamma = 1.0$ and $\omega_c = 50.0$ (exponential cut-off Eq. (5)). The QUAPI parameters are $M = 3$, $K = 6$, $\Delta t = 0.2$ (dashed line) and $M = 5$, $K = 4$, $\Delta t = 0.25$ (dashed-dotted line). The asterisks mark the initial variances $\sigma_{xx}^0 = 0.45$, $\sigma_{pp}^0 = 0.55$ and $\sigma_{xp}^0 = 0$.

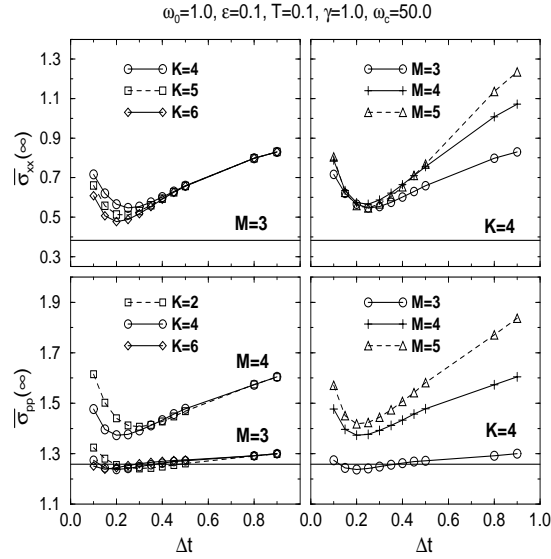


FIG. 6. Time-averaged asymptotic values of the position (upper row) and momentum (lower row) variances $\bar{\sigma}_{xx}(\infty)$ and $\bar{\sigma}_{pp}(\infty)$, respectively, versus time-step Δt for different combinations of the QUAPI parameters M and K , small driving amplitude $\epsilon = 0.1$ and bath parameters $T = 0.1$, $\gamma = 1.0$, $\omega_c = 50.0$ (exponential cut-off Eq. (5)). For the left column figures, the number M of basis states is fixed to $M = 5$ and the memory length K is varied, while for the right column figures, K is fixed to $K = 3$ and M is varied. The oscillator frequency is $\omega_0 = 1.0$.

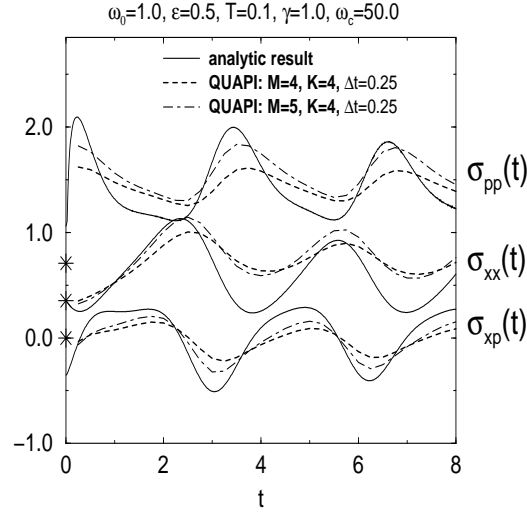


FIG. 7. Same as Fig. 5, but for the strongly driven case $\epsilon = 0.5$. Here, the QUAPI parameters are $M = 4, K = 4, \Delta t = 0.25$ (dashed line) and $M = 5, K = 4, \Delta t = 0.25$ (dashed-dotted line). The asterisks mark the initial variances $\sigma_{xx}^0 = 0.35$, $\sigma_{pp}^0 = 0.71$ and $\sigma_{xp}^0 = 0$.

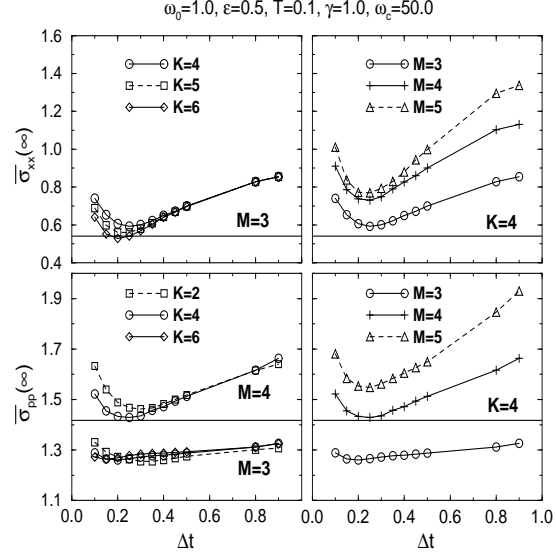


FIG. 8. Same as Fig. 6, but for the strongly driven case $\epsilon = 0.5$.

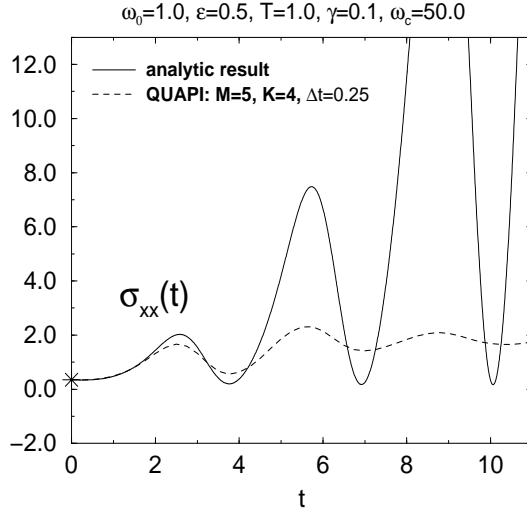


FIG. 9. Time-dependence of the position variance $\sigma_{xx}(t)$ for a parameter set where the classical dynamics is unstable, i.e. $\epsilon = 0.5, \gamma = 0.1$. The temperature is $T = 1.0$ and $\omega_c = 50.0$ (exponential cut-off Eq. (5)). The QUAPI parameters are $M = 5, K = 4, \Delta t = 0.25$. The asterisk marks the initial variance $\sigma_{xx}^0 = 0.35$. The oscillator frequency is $\omega_0 = 1.0$.

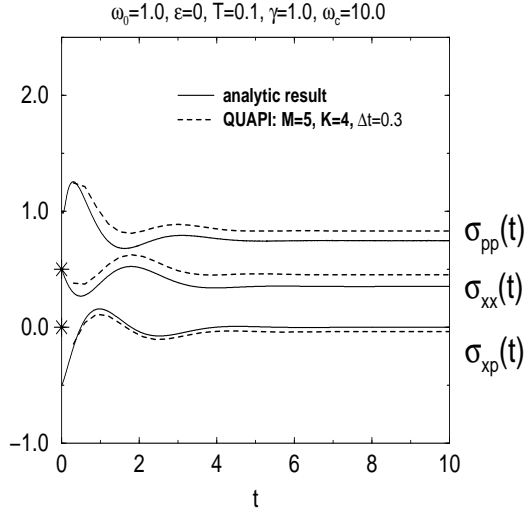


FIG. 10. Time-dependence of the variances $\sigma_{xx}(t), \sigma_{xp}(t)$ and $\sigma_{pp}(t)$ for a small cut-off frequency $\omega_c = 10.0$ (exponential cut-off Eq. (5)), $\omega_0 = 1.0, \epsilon = 0, \gamma = 1.0$ and $T = 0.1$. Here, the QUAPI parameters are $M = 5, K = 4, \Delta t = 0.30$. The asterisks mark the initial variances $\sigma_{xx}^0 = \sigma_{pp}^0 = 0.5$ and $\sigma_{xp}^0 = 0$.

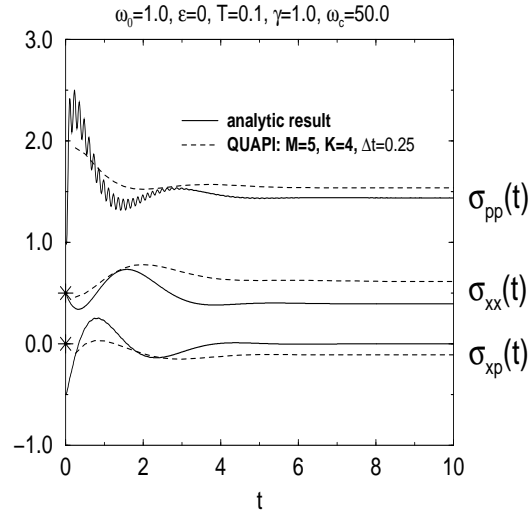


FIG. 11. Same as Fig. 3, but for a step-like cut-off Eq. (6) with $\omega_c = 50.0$. Parameters are $\omega_0 = 1.0, \epsilon = 0, T = 0.1$ and $\gamma = 1.0$. The QUAPI parameters are $M = 5, K = 4, \Delta t = 0.25$. The asterisks mark the initial variances $\sigma_{xx}^0 = \sigma_{pp}^0 = 0.5$ and $\sigma_{xp}^0 = 0$.